COBEM 2023 27TH INTERNATIONAL CONGRESS OF MECHANICAL ENGENEERING

ABCM Brazilian Society of Mechanical Sciences and Engineering
27th ABCM International Congress of Mechanical Engineering
December 04-08, 2023, Florianópolis-SC, Brazil

COB-2023-1036
SCRAMJET THRUST ANALYSIS BASED ON THE VARIATION OF ITS COMPRESSION SECTION ANGLE

Laura Carolina Monteiro dos Santos Rodrigues da Silva
Instituto Tecnológico de Aeronáutica/ITA. Programa de Pós-Graduação em Ciência e Tecnologias Espaciais. Praça Marechal Eduardo Gomes, 50 – Vila das Acácias, CEP 12228-900, São José dos Campos/SP, Brasil
lauracarolinamsr@gmail.com

Valéria Serrano Faillace Oliveira Leite
Instituto de Estudos Avançados, Trevo Coronel Aviador José Alberto Albano do Amarante, n° 1, São José dos Campos- SP
valeriavsfol@fab.mil.br

Abstract. *Supersonic combustion ramjet (scramjet) propulsion systems have been presented as an alternative to rocket engine for access to space. A methodology was developed in order to investigate the behavior of the net thrust generated by the scramjet engine by changing the angle of a single ramp of the compression section. A two-dimensional scramjet vehicle with planar symmetry is presented in this work. The oblique shock wave theory is adopted to calculate the properties in the compression section. Rayleigh's theory is considered in the combustor to consider the heat addition considering a constant area section. The area ratio theory is applied in the expansion to calculate the properties at the scramjet exit. In this work, viscous effects are not considered, and two approaches are applied: calorically perfect gas and gas in chemical and thermodynamic equilibrium. A vehicle flying at a speed equal to Mach 6 and altitude of 30 km is considered in this analysis. As a result, the first ramp angle variation in relation to an initial geometry that maximizes the mass flow results in the decrease of scramjet performance. However, the methodology can be effective for vehicles operating at multiple altitudes.*

Keywords: *scramjet engine hypersonic flow, oblique shock wave.*

1. INTRODUCTION

In the search for a more efficient and affordable way to access space, the supersonic combustion ramjet (scramjet) propulsion systems have been considered as an alternative to the rocket propulsion systems, since the transport of oxidant is unnecessary in the dense atmosphere, which results in an improvement in the capacity to carry payload (Om Prakash Raj and Venkatasubbaiah, 2012). As this is a technology still under development, new tools, and theories for the studies of the vehicle geometry are important to contribute to evaluate the behavior of the thermodynamics properties of the air regarding changes in the geometric variables. Currently, the development of scramjet propulsion technology arouses the interest of several nations around the world, including the USA, Australia, Russia, Japan, France, Germany, India, and more recently Brazil.

The hypersonic airbreathing propulsion technology is one of the most promising for high-speed transportation, due to its efficiency, resulting from the absence of complicated moving parts and, as mentioned, the absence of oxidants (Preller and Smart, 2017). Scramjet engines offer substantial advantages in terms of performance when compared to other aerospace vehicles operating at hypersonic speed through the Earth's low atmosphere (up to 70 km of altitude). As a matter of fact, considering a rocket engine and a scramjet vehicle, both using H_2 as fuel, a typical specific impulse value for a rocket engine is 500 s, from launch to Earth's low orbit with a Mach number of 20, while for the scramjet, the specific impulse is 3500-500 s, considering Mach numbers from 6 to 20 respectively (Carneiro et al., 2022).

One of the factors that contribute to the success of airbreathing hypersonic vehicles is the complete integration between the engine and the airframe, in order to reduce the overall drag and achieve positive thrust margins (O'Neill and Lewis, 1992). This high level of integration is important because the front section of the vehicle contributes to the atmospheric air compression. Scramjet vehicles operate according to the following steps: (a) the flow at hypersonic speed is compressed through the intake until it reaches the desired temperature and pressure; (b) fuel is injected into the compressed airflow and the gas mixture is ignited and combusted at supersonic speed; (c) the gas expands and is accelerated through the nozzle, in order to generate thrust (Fujio and Ogawa, 2021).

According to Heiser and Pratt (1994), ramjets are engines without moving parts (without rotating components) designed to operate in a speed range from Mach 3 to 6, operating based on the Brayton cycle. The surfaces of the vehicle itself are responsible for compressing the flow through oblique shock waves, with a normal shock wave at the end, so that the flow reaches subsonic speed in the combustor. When the air flow has a Mach number greater than 6, the deceleration process results in very high pressure and temperature in the combustor, causing the decomposition of air molecules,

without combustion occurring. At this operating speed, the engine becomes a drag device. In order to avoid this problem, the alternative is that the compression is carried out exclusively through oblique shock waves, and the flow is supersonic throughout the device, featuring an airbreathing propulsion system known as a supersonic combustion ramjet- scramjet, which presents better performance for flights with Mach numbers above 6 (Curran, 2001).

Heiser and Pratt (1994) present commonly used terminology to name the different design features of the scramjet with a mixed compression section (Figure 1). In this case, the scramjet is divided into three main components: compression section, combustor, and expansion section, with the compression and expansion sections divided into internal and external sections. Stations 0 and 1 correspond to the vehicle and cowl leading-edges, respectively. Stations 3 and 4 are the combustor inlet and exit. And stations 9 and 10 correspond, respectively, to the trailing-edges of the cowl and vehicle.

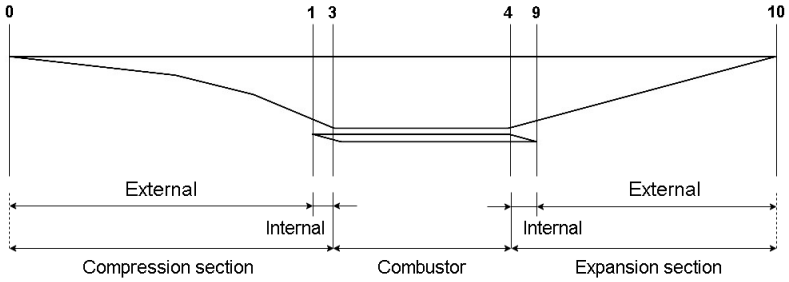

Figure 1. Airframe-integrated scramjet stations.

In order to design aerospace systems, it is common to develop simplified tools capable of identifying project requirements and need and, in some cases, defining preliminary configurations in order to highlight the existence of problems and serve as a basis for future systems.

Bonelli et al. (2011) describe the modeling of a computational tool, called SPREAD 2.0, used in the preliminary design of a hypersonic vehicle, considering the presence of oblique shock waves, fuel mixture and combustion sections and expansion section. Soares et al. (2021) developed a tool for the preliminary design of hypersonic airbreathing vehicles, using scramjet technology. Assuming a planar geometry and the hypothesis of perfect gas and inviscid flow, the model was sectioned into inlet, combustion and expansion sections, applying the respective theoretical-analytical analyzes of each section.

The main purpose of this paper is to analyze the influence in the provide vehicle thrust, at its exit, by moving a single ramp at its frontal section, considering a planar symmetry scramjet vehicle with a mixed compression system.

2. METHODOLOGY

In order to analyze thrust generated by modifying the geometry of the compression section of the scramjet, this study considers the variation of the angle of the first inlet ramp of a pre-calculated geometry, to investigate the impact on the thermodynamic properties at the combustor inlet, and in the decrease of the mass flow. The theories used to calculate properties along the scramjet are described in this section.

2.1 Compression section

For the design of the compression section, the oblique shock wave theory is applied, in order to ensure that the freestream airflow is compressed and achieves the thermodynamic properties and velocity necessary at the combustor for a supersonic combustion and thrust generation, as the vehicle reaches higher flight velocity.

According to Anderson (2003), oblique shocks waves occur when a supersonic or hypersonic flow is deflected with respect to the direction of the incoming flow, remaining parallel to the surface. In the frontal region of the wedge, an oblique shock wave is established.

Considering the simplifications of one-dimensional, stationary, adiabatic, and inviscid flow, and disregarding body forces, the equations of continuity, momentum, and energy lead to a set of algebraic equations that relate gas properties before and after the oblique shock, as presented by Anderson (2003). The relation between the surface angle θ, the oblique shock wave angle β, and the Mach number of the incident shock wave M, known as the $\theta - \beta - M$ relation is also presented by Anderson (2003). The equations that relate the flow properties, Mach number and ramp angle are given by Eq. (1) to (7).

$$\tan\theta = 2\cot\beta\left[\frac{M_1^2\sin^2\beta - 1}{M_1^2(\gamma + \cos 2\beta) + 2}\right], \tag{1}$$

$$M_{n1} = M_1 \sin\beta, \tag{2}$$

$$\frac{\rho_2}{\rho_1} = \frac{(\gamma+1)M_{n1}^2}{(\gamma-1)M_{n1}^2+2}, \tag{3}$$

$$\frac{p_2}{p_1} = 1 + \frac{2\gamma}{\gamma+1}(M_{n1}^2 - 1), \tag{4}$$

$$\frac{T_2}{T_1} = \frac{p_2}{p_1}\frac{\rho_1}{\rho_2}, \tag{5}$$

$$M_{n2}^2 = \frac{M_{n1}^2+[2/(\gamma-1)]}{[2\gamma/(\gamma-1)]M_{n1}^2-1}, \tag{6}$$

$$M_2 = \frac{M_{n2}}{\sin(\beta-\theta)}, \tag{7}$$

where ρ, p, T, and M_n represent the density, pressure, temperature and normal component of Mach number, respectively. And indices 1 and 2 correspond to the conditions before and after the oblique shock wave.

2.2 **Combustor**

For the combustion process to occur, it is necessary that the flow that enters the scramjet combustor has supersonic speed ($M > 1$) and the temperature, and Mach number must be high enough for the fuel to self-ignite. The flow must transfer heat in order to heat the fuel up to the spontaneous ignition temperature. For the case of hydrogen as fuel, it is assumed that the temperature at the combustor inlet must be greater than or equal to 900 K and the Mach number around 2, since the auto-ignition temperature of hydrogen is 845.15 K, according to CRC (1983).

In this simplified methodology, the addition of fuel mass is disregarded, and combustion is modeled by one-dimensional flow with heat addition theory, known as Rayleigh flow theory. Considering the known properties at the combustor inlet and assuming the requirement that the flow must remain supersonic at the end of the process ($M = 1{,}1$), the properties at the combustor exit can be calculated from the equations presented by Anderson (2003) and given by Eq. (8) to (10).

$$\frac{p_4}{p_3} = \frac{1+\gamma M_3^2}{1+\gamma M_4^2}, \tag{8}$$

$$\frac{T_4}{T_3} = \left(\frac{1+\gamma M_3^2}{1+\gamma M_4^2}\right)^2 \left(\frac{M_4}{M_3}\right)^2, \tag{9}$$

$$\frac{\rho_4}{\rho_3} = \left(\frac{1+\gamma M_3^2}{1+\gamma M_4^2}\right)\left(\frac{M_3}{M_4}\right)^2, \tag{10}$$

where indices 3 and 4 correspond to the properties at the combustor inlet and exit, respectively.

2.3 Expansion section

After the supersonic combustion products exiting the combustor, when experiencing a negative deflection angle, an expansion wave is established. The properties of the flow can be found through the area ratio theory, based on the relations presented by Anderson (2003), once the expansion ramp angle is known.

Once the expansion process takes place, it is possible to calculate the net thrust generated by the engine, this being the thrust generated disregarding the presence of drag, which can be calculated from Eq. (11) (Heiser and Pratt, 1994).

$$\mathrm{F} = \dot{m}_{10}u_{10} - \dot{m}_0 u_0 + (p_{10} - p_0)A_{10}, \tag{11}$$

where $\dot{m}$ is the mass flow, u is the flow velocity, p is the pressure and A is the area. The indices 0 and 10 correspond to stations 0 and 10 of the scramjet, as shown in Figure 1.

2.4 Calorically perfect air and equilibrium air

The relations adopted for the calculation of the properties through the scramjet vehicle depend on the variable γ, which is the ratio between the specific heat at constant pressure, c_p, and at constant volume, c_v, this being dependent on the chemical composition of the gas.

The calorically perfect gas is one in which the values of c_p e c_v can be considered constant, so the value of γ is also constant. This case is applied in order to simplify the calculations, however, for cases where there is a large increase in temperature, a study that considers this impact is necessary.

Air in thermodynamic equilibrium is the case in which the chemical composition of each point in the flow is determined by the temperature and pressure at that point. This case takes into account the temperature lost due to the dissociation of molecules present in the flow. Tannehill and Mugge (1974) present a practical calculation method for atmospheric air, used to insert the properties of the air in equilibrium in the calculations of the flow equations.

In this study, the impact on the calculated thrust value is evaluated considering the simplification of calorically perfect air, when compared with equilibrium air.

2.5 Initial geometry

In order to evaluate the impact of varying the angle of a compression ramp, it is first necessary to define the geometry that will be used as the basis for the calculations. For the definition of this geometry, theories are applied in order to obtain a better vehicle performance. Martos (2017) defines the optimal number of compression ramps as three, analyzing the relation between the number of ramps and the compression efficiency.

The optimization criterion applied to a mixed supersonic inlet system (Oswatitsch, 1947; Ran and Mavris, 2005) results in a constant shock intensity through the compression system. This criterion is used in order to maximize the total pressure recovery and results in the relation shown in Eq. (12).

$$M_0 \sin\beta_1 = M_1 \sin\beta_2 = M_{n-2} \sin\beta_{n-1}, \tag{12}$$

where n is the number of ramps in the compression section.

In order to maximize the air capture area, and consequently maximize the mass flow, the incident shock waves must hit the cowl leading-edge, characterizing on-lip shock, while the reflected shock wave must hit the entrance of the combustor, featuring on-corner shock.

The area of station 10 of the scramjet is defined considering that the pressure in that station is equal to the ambient pressure, characterizing a perfectly expanded nozzle.

With these considerations it is possible to define the geometry that will serve as a basis for the thrust evaluation for different angles of the first compression ramp.

2.6 Mass flow loss

Considering that the initial geometry is designed so that all shock waves hit the cowl leading-edge, when changing the angle of the first compression ramp, it is possible that there is a reduction in the mass flow when the angle used is greater than the projected angle. Figure 2 shows the case in which the incident wave on the first ramp does not hit the cowl leading-edge, resulting in a reduction in the mass flow.

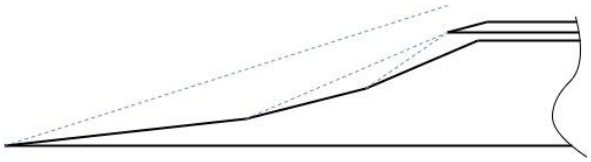

Figure 2. Configuration of shock waves resulting in loss of mass flow.

For the purpose of calculating the loss of mass flow, it is necessary to analyze two possible cases. The first one is where the loss of mass flow occurs in the first compression ramp. In this case, the methodology used is represented in Figure 3 and explained below.

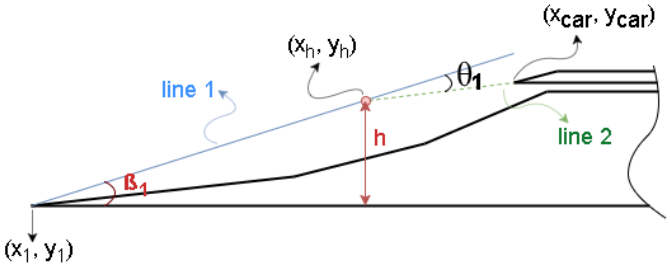

Figure 3. Configuration of mass flow loss in the first ramp.

In order to calculate the mass flow after the first shock, it is necessary to find the heigh, h, perpendicular to the flow before the shock. This height can be calculated from the difference between the y coordinates of the intersection point of lines 1 and 2 and the vehicle leading-edge. The equations of lines 1 and 2 are presented by Eq. (13) and Eq. (14), respectively.

$$y = (\tan\beta_1)x + y_1 - x_1 \tan\beta_1, \tag{13}$$

$$y = (\tan\theta_1)x + y_{car} - x_{car} \tan\theta_1, \tag{14}$$

where x_{car} and y_{car} are the cowl leading-edge coordinates.

The x coordinate of the intersection point of the lines can be found by solving the equations of lines 1 and 2. The x and y coordinates are then given by Eq. 15 and Eq. 16, respectively.

$$x_h = \frac{y_{car} - x_{car}\tan\theta_1 - y_1 + x_1\tan\beta_1}{\tan\beta_1 - \tan\theta_1}, \tag{15}$$

$$y_h = (\tan\beta_1)\left[\frac{y_{car} - x_{car}\tan\theta_1 - y_1 + x_1\tan\beta_1}{\tan\beta_1 - \tan\theta_1}\right] + y_1 - x_1\tan\beta_1, \tag{16}$$

Figure 4 shows the case in which the loss of mass flow occurs in the other compression ramps.

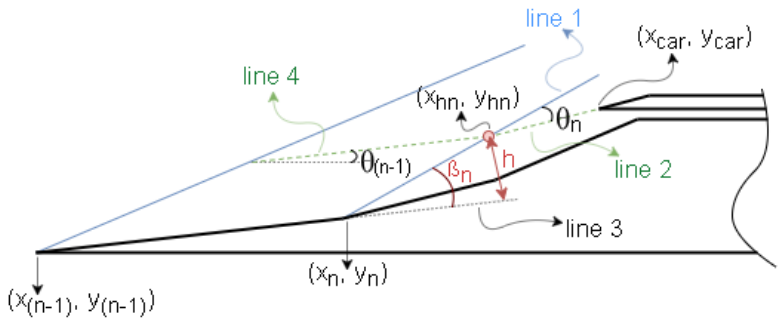

Figure 4. Configuration of mass flow loss in the other ramps.

The calculation of the loss of mass flow in the other ramps requires more steps, the first being the definition of the intersection point of lines 1 and 2, following the same steps used for the first ramp. The equation of lines 1, 2 and 3 are presented by Eq. (17), (18) and (19), respectively.

$$y = [\tan(\beta_n + \textstyle\sum_{i=1}^{n-1}\theta_i)]x + y_n - x_n \tan(\beta_n + \textstyle\sum_{i=1}^{n-1}\theta_i), \tag{17}$$

$$y = [\tan(\textstyle\sum_{i=1}^{n}\theta_i)]x + y_{car} - x_{car} \tan(\textstyle\sum_{i=1}^{n}\theta_i), \tag{18}$$

$$y = [\tan(\textstyle\sum_{i=1}^{n-1}\theta_i)]x + y_n - x_n \tan(\textstyle\sum_{i=1}^{n-1}\theta_i), \tag{19}$$

After defining the point of intersection between lines 1 and 2, it is possible to find the equation of line 4.

$$y = [\tan(\textstyle\sum_{i=1}^{n-1}\theta_i)]x + y_{hn} - x_{hn} \tan(\textstyle\sum_{i=1}^{n-1}\theta_i), \tag{20}$$

The height perpendicular to the flow can be calculated from the distance between lines 3 and 4 that have the same angle.

$$h = \frac{|\tan(\sum_{i=1}^{n-1}\theta_i)\times x_{hn} + (-1)\times y_{hn} + y_n - x_n\tan(\sum_{i=1}^{n-1}\theta_i)|}{\sqrt{(\tan(\sum_{i=1}^{n-1}\theta_i))^2 + (-1)^2}}, \tag{21}$$

From the perpendicular height, it is possible to calculate the mass flow, considering the corrected area.

3. RESULTS AND DISCUSSIONS

In order to analyze the developed methodology, operating parameters of the scramjet vehicle were defined. The adopted Mach number and flight altitude are presented in Table 1, as well as the pre-defined geometric parameters and the requirements at the combustor inlet.

Table 1. Predefined scramjet analysis parameters.

Description	Symbol	Value	Unit
Flight Mach number	M_0	6	-
Geometric flight altitude	Z	30000	m
Vehicle width	W	0.15	m
Vehicle height	H	0.40	m
Expansion ramp angle	θ_{exp}	15	º
Mach number at the combustor inlet	M_3	≥ 2	-
Temperature at the combustor inlet	T_3	≥ 900	K

The thermodynamic properties of atmospheric air at the altitude under analysis are calculated according to the model presented in US Standard Atmosphere (1976).

Table 2. Thermodynamic properties of atmospheric air at an altitude of 30 km.

Description	Symbol	Value	Unit
Temperature	T_0	226.51	K
Pressure	p_0	0.01841	kg/m³
Density	ρ_0	1197.03	Pa
Sound speed	a_0	301.71	m/s
Flight speed	V_0	1810.25	m/s

3.1 Calorically perfect air X equilibrium air

With the objective of analyzing the errors due to the use of the hypothesis of calorically perfect air when compared with equilibrium air, a geometry was defined applying the concepts presented in sections 2.4 to 2.5, considering calorically perfect air. The geometry obtained was then studied applying the methodology of Tannehill and Mugge (1974), presented in section 2.4, for the calculation of γ and temperature.

The inlet geometry and its properties are presented in Table 3, for the two cases under analysis.

Table 3. Geometry and properties of the scramjet considering calorically perfect and equilibrium air.

Position	γ	$T\ [K]$	$p\ [Pa]$	$\rho\ [kg/m^3]$	$M\ [-]$	$V\ [m/s]$
Calorically perfect air						
1st ramp $\theta_1 = 6.18°$	1.4	293.75	2796.67	0.03317	5.16	1772.54
2nd ramp $\theta_2 = 7.16°$	1.4	380.96	6533.94	0.05975	4.40	1722.40
3rd ramp $\theta_3 = 8.35°$	1.4	494.06	15265.46	0.10764	3.71	1665.11
Combustor inlet	1.4	900.00	80528.06	0.31170	2.31	1386.98
Combustor exit	1.4	2012.57	252472.08	0.43702	1.10	989.27
Vehicle exit	1.4	436.23	1197.03	0.00956	4.86	2036.19
Net thrust $F[N]$				451.80		
Equilibrium air						
1st ramp $\theta_1 = 6.18°$	1.4	293.75	2796.67	0.03317	5.16	1772.54
2nd ramp $\theta_2 = 7.16°$	1.4	380.96	6533.94	0.05975	4.40	1722.40
3rd ramp $\theta_3 = 8.35°$	1.4	494.06	15265.46	0.10764	3.71	1655.11
Combustor inlet	1.379	867.20	79127.90	0.31473	2.34	1373.64
Combustor exit	1.344	1947.86	252380.09	0.44753	1.10	1151.94
Vehicle exit	1.4	422.21	1196.59	0.00979	4.86	2003.01
Net thrust $F[N]$				385.39		

Some information can be observed through the data in Table 3. The first factor to consider is the fact that the flow behaves as calorically perfect until the reflected shock that occurs before the combustor inlet. Thus, there is only variation in γ after the reflected shock wave, resulting in a consequent reduction in temperature, since the consideration of equilibrium air takes into account the energy spent on the dissociation of molecules.

It is possible to note that the geometry obtained assuming calorically perfect air is not capable of achieving the necessary properties at the combustor inlet for self-ignition to occur, when analyzed assuming equilibrium air. In addition, the pressure at the exit of the vehicle is lower than atmospheric air pressure, which may result in a choked flow.

3.2 Initial geometry

The initial geometry to be used for the analysis of the variation of the angle of the first compression ramp is defined from the methodology presented in section 2, considering equilibrium air and the parameters and properties presented in Tables 1 and 2.

The angles for the compression ramps, as well as the properties along the scramjet vehicle are presented in Table 4. From the data obtained, it is possible to notice that this configuration of angles of the compression section is able to reach the necessary requirements in the combustor inlet, with a temperature equal to 900 K and a Mach number around 2. In order for the temperature requirement to be met, it was necessary that the angles of the compression ramps were greater than the angles obtained for the calorically perfect case, since part of the temperature is transferred to the dissociation process of the molecules.

Table 4. Geometry and properties of initial vehicle under analysis.

Position	γ	$T\ [K]$	$p\ [Pa]$	$\rho\ [kg/m^3]$	$M\ [-]$	$V\ [m/s]$
1st ramp $\theta_1 = 6.41°$	1.4	296.81	2879.27	0.03380	5.13	1770.84
2nd ramp $\theta_2 = 7.48°$	1.4	388.85	6925.63	0.06206	4.34	1717.83
3rd ramp $\theta_3 = 8.78°$	1.4	509.44	1665.85	0.11394	3.64	1645.81
Combustor inlet	1.378	900.00	88912.70	0.33870	2.24	1311.97
Combustor exit	1.346	1905.21	262725.35	0.47629	1.10	1106.63
Vehicle exit	1.4	411.88	1197.03	0.01013	4.90	1992.03
Net thrust $F[N]$				345.26		

The heigh obtained for the combustor was calculated considering that the mass flow is constant along the vehicle and is equal to 0.0147 m. For this project, the combustor height was considered equal to 0.015 m.

3.3 Angle variation

Based on the geometry obtained in section 2, the angle of the first compression ramp has been modified from 6º to 7°, in order to evaluate the impacts on thrust generation.

Figure 5 shows the mass flow variation according to the variation of the angle of the first ramp. For angles lower than the initial design angle of 6.40°, the mass flow remains constant, since the shock waves hit the interior of the cowl, despite not hitting its leading-edge. When the angles are greater than the design angle, the mass flow tends to decrease, since the shock waves stop hitting the cowl.

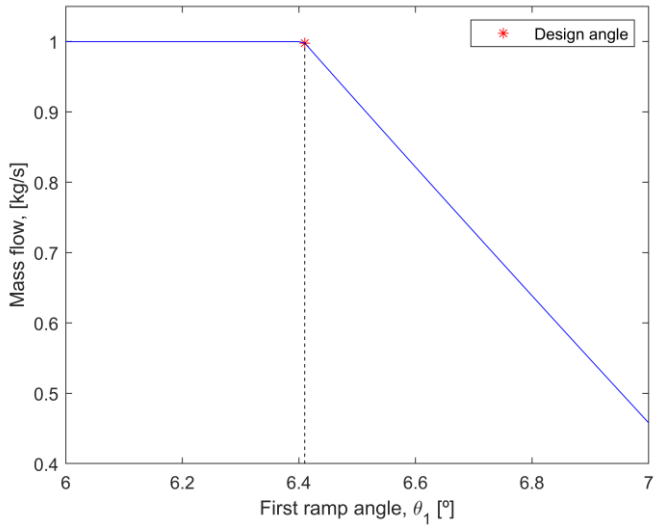

Figure 5. Mass flow variation.

Table 5 presents the mass flow values after each shock wave for angles greater than the design angle, in order to assess its decay. It is possible to observe that for the design angle the mass flow remains constant throughout the shocks, while for the higher angles, there is loss of mass flow with each shock wave.

Table 5. Variation of mass flow at each ramp.

Angle	**Mass flow** $[kg/s]$		
	1st ramp	**2nd ramp**	**3rd ramp**
Design angle $\theta_1 = 6.40°$	0.9998	0.9998	0.9998
$\theta_1 = 6.41°$	0.9997	0.9991	0.9977
$\theta_1 = 6.70°$	0.9848	0.9112	0.7298
$\theta_1 = 7.00°$	0.9676	0.8197	0.4581

In order to evaluate the impact of the angle variation on the mass flow reduction, Table 6 presents a comparison between the angles and the mass flows of each angle in relation to de initial design. In addition, the same table shows the percentage change in mass flow at each shock wave.

Table 6. Percentage variation of angles and mass flows.

Angle	**Variation** [%]				
	Design angle		**Mass flow through the ramps**		
	Angle	**Mass flow**	**1st to 2nd**	**2nd to 3rd**	**1st to 3rd**
$\theta_1 = 6.41°$	0.16	-0.21	-0.06	-0.14	-0.20
$\theta_1 = 6.70°$	4.69	-27.00	-7.47	-19.91	-25.89
$\theta_1 = 7.00°$	9.38	-54.18	-15.29	-44.11	-52.65

From Table 6, it is possible to notice that, with the increase of the angle of the first ramp, the percentage decrease of the mass flow at each shock increases. This shows that small variations in the angle of the ramp can result in a significant reduction in the mass flow, since for an angle variation lower than 10%, there is a reduction in the mass flow greater than 50%.

In order to verify the accuracy of the analytical calculations of mass flow loss, the vehicle was modeled and analyzed using the ANSYS – Fluent 19.2 CFD code. To nullify the boundary effects in the simulation, it was considered a domain larger than the vehicles dimensions. Since it is a 2D inviscid analysis, a general mesh with triangular elements with a maximum size of 5 mm was considered. Considering the geometry of the compression section with angles of 7.00°, 7.48° and 8.78° for the first, second and third ramps, respectively, Figure 6 shows the analysis used domain and the considered boundary conditions. From the defined surfaces, the size of the elements grows from a rate of 1.0125, until the entire space of the domain is contemplated, resulting in a number of nodes of 15529.

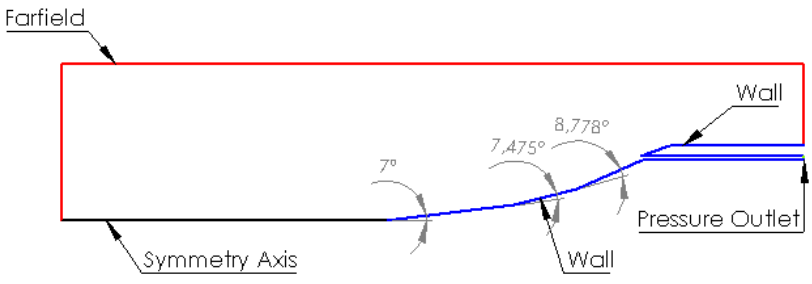

Figure 6. Analysis domain and boundary conditions.

Figure 7 shows the variation of the Mach number for each shock wave, which shows the reduction of the Mach number until it reaches the required conditions at the combustor inlet.

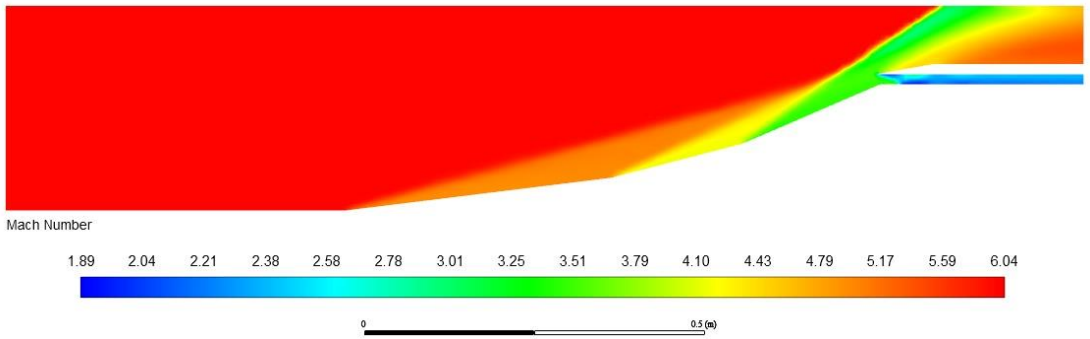

Figure 7. Mach number results of numerical analysis.

From the numerical analysis, a mass flow of 0.4557 kg/s was obtained inside the combustion chamber, while the calculated mass flow was equal to 0.4581 kg/s, demonstrating that the mathematical model used to calculate the mass flow loss presents a result consistent with the physical phenomenon represented.

Figure 8 shows graphs of the temperature and Mach number at the combustor inlet and the pressure at the vehicle exit. From the graph that presents the temperature values at the combustor inlet, it is possible to notice that for angles smaller than the design angle, the temperature is not high enough for the fuel to self-ignite. In this case, for the ramp variation to be possible for smaller angles, it is necessary that the initial geometry be designed for temperatures higher than the defined 900 K. Observing the graph of the pressure at the scramjet exit, it is noted that again for angles lower than the design, the vehicle is not able to reach the necessary requirements, in this case, a pressure equal to or greater than atmospheric pressure, so that the choked flow does not occur.

From the Mach number graph, two possible problematic situations for vehicle operation can be observed. The first one is the reduction of the Mach number with the increase of the angle. In the case of the interval under analysis, the Mach number is not below 2, however the behavior shows that the Mach number can reach this value with the increase of the angle. The second possible problem is the reduction of the Mach number with decreasing angle. This factor is relevant since the flow cannot be at a very high velocity so that it can remain in the combustor long enough for the combustion process to occur.

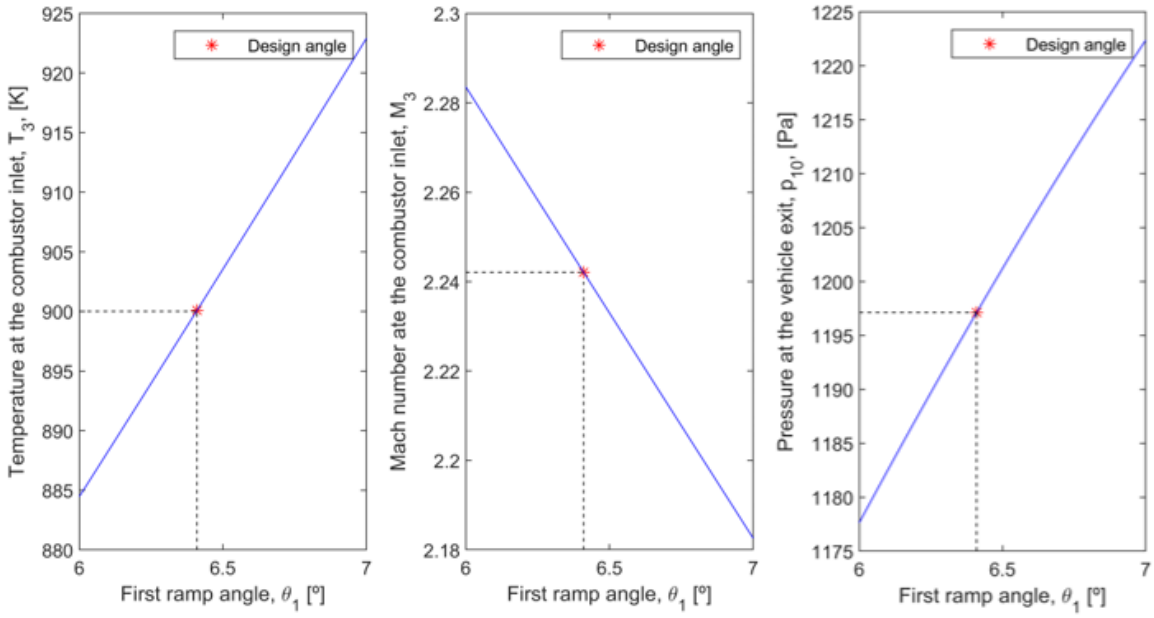

Figure 8. Temperature and Mach number at the combustor inlet and pressure at the scramjet exit.

Figure 9 shows the net thrust behavior with the variation of the first ramp angle. From the graph, it is possible to see that the thrust decreases with the increase of the angle. However, the decrease occurs for different reasons for the angles above and below the design angle. For angles greater than the design angle, the reduction in the net thrust is due to the loss of mass flow, since the mass flow decreases with increasing angle, as shown in Figure 5. For angles smaller than the

design angle, it is necessary to analyze Eq. (11). Despite the pressure at the vehicle exit being lower than the atmospheric pressure for these cases, it is not low enough to contribute negatively to the net thrust calculation. Thus, the behavior of the net thrust can be explained by the value of the speed at the vehicle exit, which is higher as function of the Mach number at the combustor inlet, disregarding the time necessary for the combustion to occur.

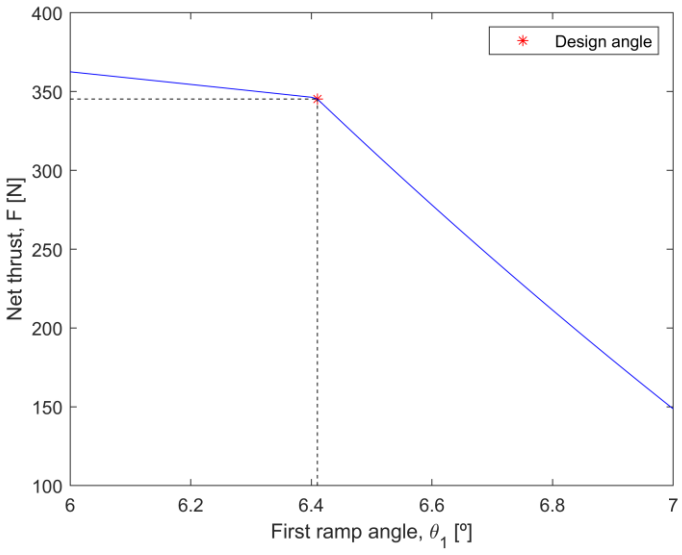

Figure 9. Variation of net thrust.

4. CONCLUSION

A generic scramjet geometry was designed using analytical theoretical analysis for an altitude of 30 km and a Mach number of 6, in order to analyze the behavior of the net thrust with the variation of the compression section geometry, considering the variation of the first ramp angle. In addition, the influence of the hypothesis of calorically perfect air and equilibrium air was analyzed.

From the analysis of the geometry generated considering calorically perfect air, it is possible to conclude that the hypothesis can be applied to the first compression ramps, however, with the increase in temperature, it is necessary to apply the hypothesis of equilibrium air, in order to consider the variations in the chemical composition of the flow through the vehicle.

With the reduction of the first ramp angle, a higher net thrust than the design thrust is obtained, however, this case is not possible, since the temperature is not high enough for the self-ignition process to occur. In this case, it is necessary to design a new initial geometry that reaches a temperature higher than 900 K, so that the temperature reduction does not result in temperatures below the minimum.

Increasing the first ramp angle results in a large decrease in net thrust, as it causes a reduction in mass flow. Therefore, increasing the angle results in a decrease in scramjet performance.

From the analyzes carried out, it is possible to conclude that for a vehicle operating at a constant altitude, the variation of the first ramp angle is detrimental to its performance, being more appropriate the application of the methodology that maximizes the mass flow. However, the angle variation can be beneficial for vehicles operating at different altitudes, since the angle variation can be performed in order to increase the air capture area, with the least possible variation in the vehicle geometry.

5. ACKNOWLEDGEMENTS

This study was financed in in part by the Coordenação de Aperfeiçoamento de Pessoal de Nível Superior - Brasil (CAPES) - Finance Code 001. This work was carried out with the support of the Academic Cooperation Program in National Defense (PROCAD-DEFESA), grant 88887.387752/2019-00. The authors would like to thank the Instituto Tecnológico de Aeronáutica (ITA) and the Instituto de Estudos Avançados (IEAv). Finally, the authors would like to express their thanks to Luiz Henrique Silva Marques Soares, Master's student at the Instituto Tecnológico de Aeronáutica (ITA), for assistance with the numerical analysis.

6. REFERENCES

Anderson, J. D., 2003. “Modern compressible flow: with historical perspective. McGraw-Hill Education.
Atmosphere, U. S., 1976. NASA TM-X 74335.
Bonelli, F., Cutrone, L., Votta, R., Viggiano, A., Magi, V., 2011. “Preliminary design of a hypersonic air-breathing vehicle”. 17th AIAA International Space Planes and Hypersonic Systems and Technologies Conference. AIAA-2011-2319.
Carneiro, R. Araújo, P. P. B., Marinho, G. S., et al., 2022. “Leading-to-tailing edge theoretical design of generic scramjet”. AIP Advances 12, 055322 (2022). Publication date: 13 May 2022.
CRC, Aviation Fuel Properties, 1983. “Report 530”. Coordinating Research Council, Inc.
Curran, E. T., 2001. “Scramjet engines: the first forty years”. Journal of Propulsion and Power, Vol. 17, No. 6, pp. 1138-1148.
Fujito, C., Ogawa, H., 2021. “Physical insight into axisymmetric scramjet intake design via multi-objective design optimization using surrogate-assisted evolutionary algorithms”. Aerospace Science and Technology 113 (2021) 106676. Publication date: 26 March 2021.
Heiser, W. H., Pratt, D. T., 1994. “Hypersonic airbreathing propulsion”. Washington, D. C., American Institute of Aeronautics and Astronautics.
Martos, J., 2017. “Aerothermodynamic design, manufacture and testing of a 3-D prototyped scramjet”. Doctor in science in the program of space science and technology, area of space propulsion and hypersonics, Instituto Tecnológico de Aeronáutica, São José dos Campos.
Om Prakash Raj, N., Venkatasubbaiah, K., 2012. “A new approach for the design of hypersonic scramjet inlets”. Physics of Fluids 24, 086102 (2012). Publication date: 30 august 2012.
O’Neill, M. K. L., Lewis, M. J., 1992. “Optimized scramjet integration on a waverider”. Journal of Aircraft, Vol. 29, No. 6, Nov.-Dec. 1992.
Oswatitsch, K., 1947. “Pressure recovery for missiles with reaction propulsion at high supersonic speeds (the efficiency of shock diffusers)”. NACA Technical Memorandum, Vol. 1140.
Preller, D., Smart, M. K., 2017. “Reusable launch of small satellites using scramjets”. Journal Spacecraft and Rockets 54 (6) (2017) 1317-1329.
Ran, H., Mavris, D., 2005. “Preliminary design of a 2-D supersonic inlet to maximize total pressure recovery”. AIAA 5th Aviation, Technology, Integration, and Operation Conference (ATIO), p. 11.
Soares, L. H. S. M., Araújo, P. P. B., Toro, P. G. P., Martos, J. F. A., 2021. “Modeling, implementation and application of a tool for preliminary hypersonic airbreathing vehicle design”. 26th COBEM International Congress of Mechanical Engineering. COB-2021-0495.
Tannehill, J. C., Mugge, P. H., 1974. “Improved curve fits for the thermodynamics properties of equilibrium air suitable for numerical computation using time-dependent of shock capturing methods”. NASA CR-2470, October, 1974.

7. RESPONSIBILITY NOTICE

The authorsare the only responsible for the printed material included in this paper.